Construction and Building Materials 128 (2016) 361–372

Contents lists available at ScienceDirect

Construction and Building Materials

journal homepage: www.elsevier.com/locate/conbuildmat

Mechanical and hydration characteristics of autoclaved aerated concrete (AAC) containing iron-tailings: Effect of content and fineness

Lixiong Cai [a], Baoguo Ma [a], Xiangguo Li [a,*], Yang Lv [b], Zhuolin Liu [a], Shouwei Jian [a]

[a] State Key Laboratory of Silicate Materials for Architectures, Wuhan University of Technology, Wuhan 430070, China
[b] Department of Structural Engineering, Magnel Laboratory for Concrete Research, Ghent University, Technologiepark-Zwijnaarde 904, 9052 Ghent, Belgium

HIGHLIGHTS

- Effect of iron tailing content and fineness on mechanical property of B05 grade AAC blocks was investigated.
- Effect of iron tailing content and fineness on hydrothermal synthesis products of AAC was investigated.
- The thermal and crystal characteristics were determined by using TG-DSC and 29Si-NMR analysis, respectively.

ARTICLE INFO

Article history:
Received 27 April 2016
Received in revised form 18 September 2016
Accepted 6 October 2016

Keywords:
Autoclaved aerated concrete
Iron tailing
Content
Fineness
Mechanical property
Hydrothermal synthesis products

ABSTRACT

With the objective of reducing the negative impacts on environment and utilizing the secondary resource of tailings, the possibility of preparing AAC by using iron tailing was investigated. The bulk density and compressive strength were determined to indicating the feasibility of preparing AAC blocks from iron tailing. The morphology (FESEM-EDX), mineral constituent (XRD), thermal characteristics (TG-DSC) and crystal characteristics (29Si-NMR) of hydration products of AAC samples were analyzed to demonstrate the hydration characteristics of AAC products containing iron tailings effected by iron tailing content and fineness. The results indicated that the increasing content of iron tailing has negative effect on the mechanical property of AAC, and the finer of iron tailings can effectively enhance strength of AAC blocks. The main minerals in AAC products are C-S-H gel, tobermorite, anhydrite, hydrogarnet, and some residual minerals including quartz and calcite accompanied by ferric oxide and white mica in minor quantities. The increasing content of iron tailing obviously reduces the amount of calcium silicate hydrates; meanwhile, the finer of iron tailing accelerated the decomposition of white mica during the autoclaving process and has slight negative effect on crystallinity of tobermorite. It was also suggested that Al and Mg ions in iron tailings got into the structure of tobermorite during the hydrothermal reaction. This study provided the theoretical foundation for the utilizing of iron tailings in AAC production.

1. Introduction

Autoclaved aerated concrete (AAC) is a calcium-silicate autoclaving porous material with excellent thermal insulation ability which can be used both in load bearing wall and filler wall [1–3]. To extending the range of raw materials and lower the cost of production, the feasibility of preparing AAC from industrial wastes have been proposed, such as fly ash [4], air-cooled slag [5], coal bottom ash [6], efflorescence sand [7], copper tailings [8] and carbide slag [9], etc. The mechanical properties of AAC are mainly determined by the hydration products of pore partition material and the pore characteristics [10,11].

Iron tailing is an industrial solid waste mostly result from the process of iron ore exploiting, which the production ratio is 1:2.5–3.0 to iron ore. Iron tailings almost totally piled up through the history of iron ore mining in China. From 2007 to 2011, the stockpiles of iron ore tailings increased by 2.899 billion metric tons; in 2011 in particular, approximately 806 million metric tons were generated. However, the comprehensive recycling of these tailings totaled only 307 million metric tons. The increasing quantity of cumulative iron tailing has caused severe hazard to the environmental condition [12]. The allowable disposal method for iron tailings was outdoor stacking after solidify with curing agent, which may cause soil contamination, river or groundwater pollution and potential danger. For environmental protection and sustainable development many technologies have been applied to reduce the amount of iron tailing, such as recovery [13,14], fired

* Corresponding author.
E-mail address: lxggroup@163.com (X. Li).

http://dx.doi.org/10.1016/j.conbuildmat.2016.10.031
0950-0618/

Table 1
Chemical composition of the raw materials (wt.%).

Component	SiO_2	Al_2O_3	Fe_2O_3	CaO	MgO	Na_2O	K_2O	SO_3	CO_3	Cl	Ignition loss
Silicon sand	90.21	4.51	1.24	0.40	0.10	0.27	2.54	0.03	–	0.03	0.47
Iron tailing	42.90	10.75	7.51	12.97	7.10	2.06	1.96	9.04	–	0.10	4.48
Cement	17.76	3.94	4.04	61.11	1.78	–	0.29	3.52	6.32	–	0.73
Quicklime	2.78	1.02	0.73	73.64	1.45	–	0.13	0.33	12.7	0.01	6.94

blocks [15], ceramsite [16], concrete aggregate [17], and additives in the ceramic industry [18].

Utilizing iron tailing as the primary siliceous raw material to producing AAC products in agreement with the objective of strategy of resources recycling and building energy efficiency of China. Several studies have investigated the possibility of preparing AAC from iron tailings; they mainly focused on the proposing of the optimal dry mixture proportion and the hydration products transforming during autoclaved process, and few researches involved the investigation into the effecting mechanism of hydration products on the mechanical properties. On the other hand, the former studies mainly concentrate on the preparing of B06, A3.5 level AAC samples stipulated in GB 11968-2006 [19]. Nowadays, with the promotion of building energy saving requirement, production technology of AAC products with lighter weight and higher volume porosity, which have better thermal insulation ability, were urgently demand in China.

In view of the building energy saving and waste stream reduction via recycling, a new type of lightweight AAC material (B05, A2.5 stipulated in GB 11968-2006) was developed using iron tailing as siliceous substitute material. The SiO_2 in iron tailings was used to replace silicon sand as siliceous material. The physical and mechanical properties were analyzed to determine the appropriate substitution mass ratio and mechanical grinding process of iron tailing. Meanwhile, the influence of substitution mass ratio and iron tailing fineness on the hydration products were also investigated to make understanding of the relationship between mechanical properties and hydration products.

2. Experimental

2.1. Raw materials

Raw materials contained silicon sand, iron tailing, cement, quicklime and calcium sulfate dihydrate ($CaSO_4{\cdot}2H_2O$). All the raw materials used were from the same batch to ensure the stability of the chemical compositions. The chemical component of raw materials was shown in Table 1. The parameter of true density and specific surface area of silicon sand, cement and quicklime were listed in Table 2.

Table 2
True density and specific surface area of the raw materials.

Raw materials	Silicon sand*	Cement	Quicklime
True density (g/cm^3)	2.24	3.12	2.25
BET specific surface area (m^2/g)	4.1452	4.7632	5.4325

* Silicon sand was ground for 10 mins.

Iron tailing discharged by ore-dressing machinery was sampled from the Wuhan Iron and Steel (Group) Company in China. Cement and quicklime were used as calcareous materials to provide CaO in the autoclaved hydrothermal reactions. Quicklime had 71.6% active CaO and its residue on 80 μm sieve was 9.3% with 12 min digestion time, 87 °C digestion temperature. The cement was commercial ordinary portland cement 42.5 (P.O. 42.5) provided by Hubei Yadong cement Co., Ltd. The calcium sulfate dihydrate (analytically pure) was made by Sinopharm Chemical Reagent Co., Ltd. Al powder was used as a gas producing agent for the slurry foaming, which had 80%solid content, 86%active Al content, and its coating surface on water was 5417 cm^2/g.

2.2. Procedure

The mixture proportion of each sample were shown in Table 3. The amounts of cement, quicklime and gypsum in each dry mixture were 21%, 8%, and 3%, respectively, and those of aluminium powder and water were 0.14% and 60% by mass of dry mixtures. The mass ratio substitution of iron tailing to silicon sand (MSIS) of Sample T1-T7 were 0%, 20%, 40%, 50%, 60%, 80%, 100%, respectively. The effects of iron tailing fineness on the mechanical properties of AAC blocks are investigated by maintaining the MSIS at 40% with the samples T3, T8-T11. The autoclaved curing process is heating for 2 h, holding pressure at 14 bars for 8 h and depressurization for 2.5 h.

The flow chart of preparation of raw materials and samples was shown in Fig. 1. Raw materials of each sample were weighed according to the mixture proportion of Table 3. The error of powder materials and water were controlled in ±0.2 g, and Al powder was controlled in ±0.02 g. The powder materials were thoroughly

Table 3
Mixture proportion of each sample.

Sample number [a]	Calcareous		Siliceous		Gypsum	Al powder	W/R
	Cement	Quicklime	Silicon sand [b]	Iron tailing [c]			
T 1	8%	21%	68%	0%	3%	0.14%	0.6
T 2	8%	21%	54.4%	13.6%	3%	0.14%	0.6
T 3	8%	21%	40.8%	27.2%	3%	0.14%	0.6
T 4	8%	21%	34%	34%	3%	0.14%	0.6
T 5	8%	21%	27.2%	40.8%	3%	0.14%	0.6
T 6	8%	21%	13.6%	54.4%	3%	0.14%	0.6
T 7	8%	21%	0%	68%	3%	0.14%	0.6
T 8	8%	21%	40.8%	27.2%–10min	3%	0.14%	0.6
T 9	8%	21%	40.8%	27.2%–15 min	3%	0.14%	0.6
T 10	8%	21%	40.8%	27.2%–25 min	3%	0.14%	0.6
T 11	8%	21%	40.8%	27.2%–30 min	3%	0.14%	0.6

[a] Nine pieces for each sample number.
[b] Silicon sand is ball milled for 10 mins.
[c] Iron tailings of sample T1-T7 are ball milled for 20 min, T8, T9, T10, T11 are ball milled for 10min, 15 min, 25 min, 30 min, respectively.

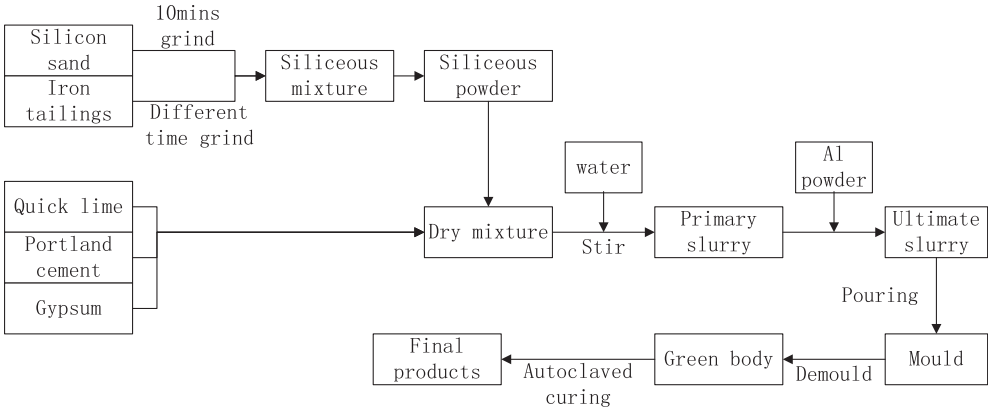

Fig. 1. Flow chart of preparation of raw materials and samples.

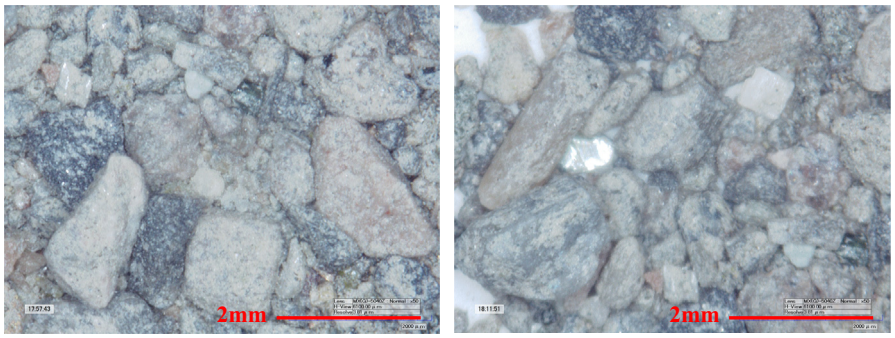

Fig. 2. Morphology of unground iron tailings magnified 50 times.

Table 4
Particle characteristics of different milling time iron tailings.

Milling time	10 mins	15 mins	20 mins	25 mins	30 mins
True density (g/cm^3)	2.794	2.886	2.941	2.986	3.093
Specific surface area (m^2/g)	2.63	3.02	4.85	5.21	5.69
Particle size <80 μm(%)	59.86	76.83	83.57	87.9	91.38

dry mixed, before adding warm water (50 ± 1 °C) and stirring for 2 min. After that, Al powder was added and mixed with the slurry for another 45 s. The ultimate slurry was poured into moulds of 100 × 100 × 100 mm^3 to forming and pre-curing at the temperature of 50 ± 2 °C for 2.5 h under a steam saturated condition. After that, cutting the swollen up surface to flat, and demoulded to getting the green body. Finally, put the green body into an industrial autoclave for hydrothermal reaction.

2.3. Characterization

2.3.1. Raw materials

The true density and specific surface area of raw materials were determined according to method stipulated in GB/T 208-2014 and GB/T 8074-2008, respectively. The particle distributions were detected by particle size analyzer, Marlvern Mastersizer 2000. The chemical components of the raw materials were determined by X-ray fluorescence spectrometer (XRF). The morphology of iron tailings were characterized by using KH-7700 digital microscope, magnified 50 times.

2.3.2. Mechanical properties

The bulk density and compressive strength were regulated by GB/T 11969-2008. In order to compare the compressive among the samples at different bulk densities, a formula for specific strength(S) was defined as $S = \sigma(MPa)/D(kg/m^3)$ (σ:tested compressive strength of the AAC samples; D: bulk density of the AAC samples).

2.3.3. Hydration products

The morphology of AAC hydration products were characterized by using JEM-2100F field-emission high resolution transmission electron microscopy (FESEM) and energy dispersive X-ray (EDX).

The mineral constituent of the iron tailing and AAC samples were detected by a D/8 Adwance X-ray diffractometer with Cu Kα radiation from 5° to 70°. The parameter of the characteristic peak of AAC samples were determined by Jade 5.0.

Thermal analysis of AAC sample was carried out with the NETZSCH STA449F3 simultaneous thermal analyzer to detect the differential scanning calorimetry (DSC) and thermogravimetric (TG) curve from 50 °C to 1000 °C.

^{29}Si solid-state nuclear magnetic resonance (NMR) analysis was conducted in a Bruker Avance III400 spectrometer operating at 79.5 MHz. The rotation frequency was 6 kHz and the delay time was 5 s.

3. Results and discussions

3.1. Characterization of iron tailings

3.1.1. Morphology

The morphology of unground iron tailing is shown in Fig. 2. It can be seen that the shape of the unground iron tailing is irregular and most of the particles are lower than 2 mm. The polychrome appearance of the particles is attributed to the metallic element in the phyllosilicate in iron tailings.

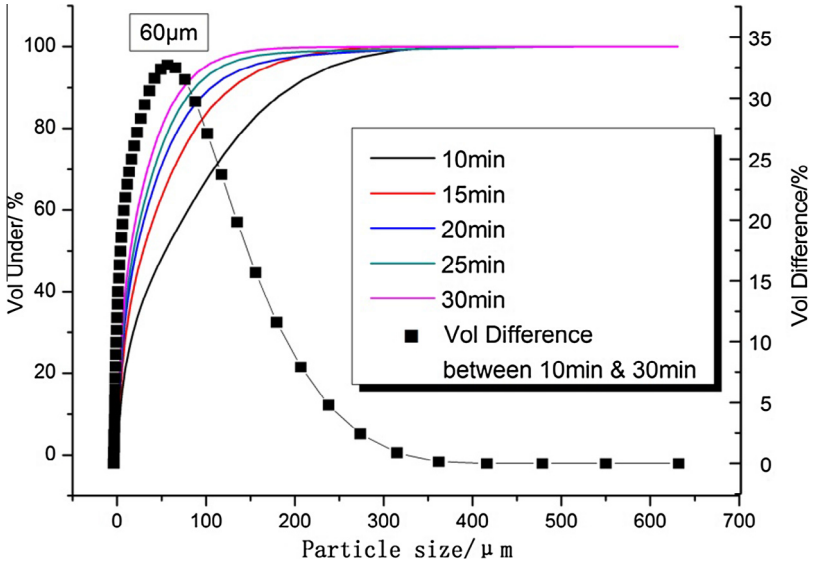

Fig. 3. Particle distribution of different milling time iron tailings.

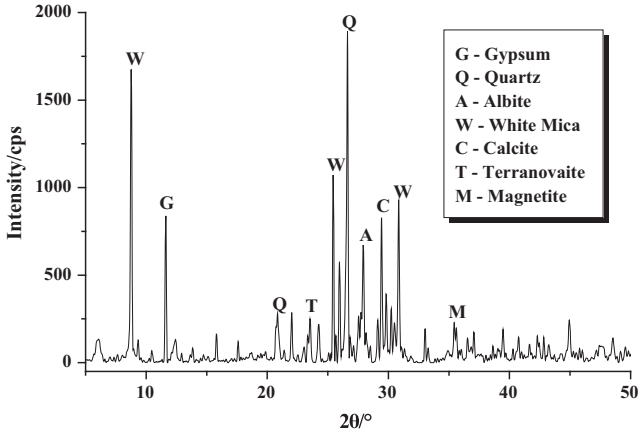

Fig. 4. XRD patterns of iron tailings.

3.1.2. Preprocessing

Mechanical grinding of the iron tailing has been used to reduce particle size and increase chemical activity when they are used as siliceous materials in AAC [20]. The true density and specific surface area of different milling time iron tailings were shown in Table 4, and the particle distribution of different milling time iron tailings are presented in Fig. 3.

The granulometry analysis of iron tailing with different grinding time showed a falling tendency in increasing milling time. The specific surface area increased from 2.63 m^2/g to 5.69 m^2/g, while the grinding time prolonged from 10 mins to 30 mins. Meanwhile, from the results of particle size distribution presented in Fig. 1, it can be seen that the percentage of the particle size below 60 μm increased mostly during the ball milling process.

3.1.3. Mineral constituent

Mineralogical analysis is carried out to identify the crystalline solid phases. The XRD pattern of iron tailing is given in Fig. 4. The pattern shown the predominant crystalline components of iron tailing are gypsum ($CaSO_4{\cdot}2H_2O$), white mica ($KAl_2Si_3AlO_{10}(OH)_2$), quartz (SiO_2) and calcite ($CaCO_3$), accompanied by minor phases including albite($(Na,Ca)Al(Si,Al)_3O_8$), terranovaite ($NaCaAl_3Si_{17}O_{40}$-H_2O) and magnetite (Fe_3O_4). The crystalline silicate phases might be beneficial for generating calcium silicate hydrate (C-S-H) gel or calcium aluminium silicate hydrate (C-A-S-H).

3.1.4. Thermal

The DSC and TG curves of 20 min ground iron tailing were presented in Fig. 5, which indicates that the iron tailing stepwisely lost weight during the heating process.

The endothermic valleys, 63.5 °C and 122.2 °C, which were related to the loss of adsorbed and bound water, respectively, accompanied with 1.6% weight loss. Keep on increasing the temperature between 150 °C and 170 °C would cause the decomposition of gypsum accompanied with slight weight loss. Two peaks of heat release appeared at 473.5 °C and 531 °C due to the oxidation reaction of organic matter in iron tailing with a 2.64% weight loss in this period. Meanwhile, the oxidation of hematite was also occurred in this temperature range, but the heat and weight variation were concealed by the stronger oxidation reaction of organic matter in iron tailing. There was a 3.76% weight loss in the sample in the temperature range of 700–1000 °C, which may be due to the decomposition of calcite into CaO at 768.5 °C [29] and dehydroxylation of white mica at 850–950 °C [30].

3.2. Mechanical property of AAC blocks

3.2.1. Effects of mass ratio substitution of iron tailing to silicon sand (MSIS)

The effects of MSIS on the mechanical properties were presented in Fig. 6. It could be seen that the bulk density presents no significant regularity by the variation of MSIS. The addition of iron tailing had no effect on the bulk density of AAC. However, with the increase of MSIS from 0% to 50%, the compressive strength slowly reduced from 3.15 MPa to 2.5 MPa; meanwhile, the specific strength decreased from 5974.6 N·m/kg to 4820.7 N·m/kg. These samples were qualified with the specification of the B05, A2.5 grade in GB 11968-2006. However, as the MSIS continue increasing to 100%, it caused a more rapid decline of compressive strength and specific strength to 1.65 MPa and 3185.3 N·m/kg, respectively. This probably attributed to the reduction of SiO_2 supplied by mixture siliceous, the main component reacting with calcium to generating C-S-H (B) and tobermorite. The reduction of C-S-H (B) and

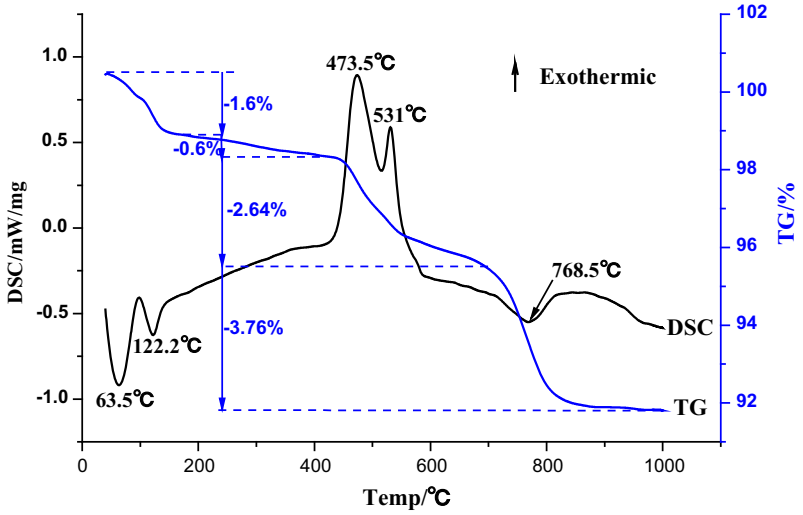

Fig. 5. TG-DSC curve of 20 min ground iron tailing.

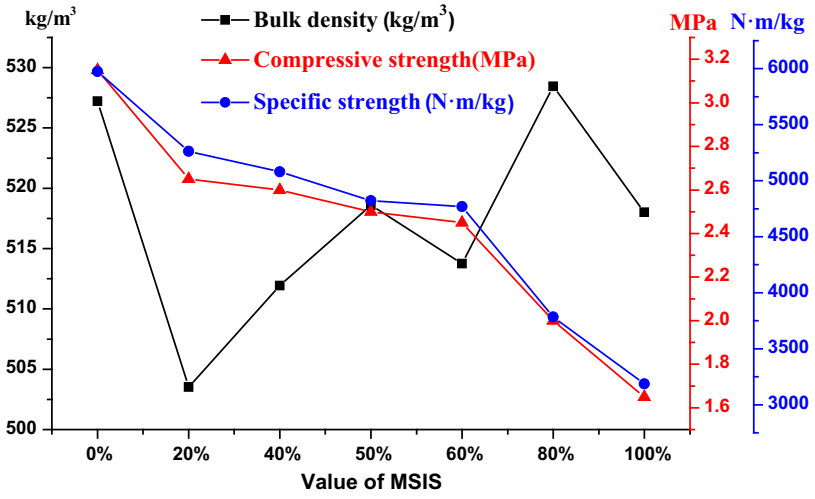

Fig. 6. Mechanical properties of AAC blocks with different MSIS.

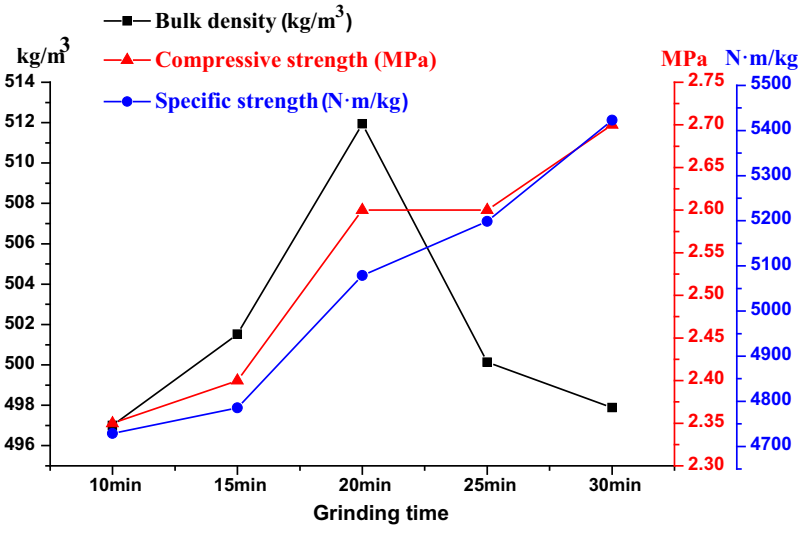

Fig. 7. Mechanical properties of AAC blocks with different fineness iron tailing.

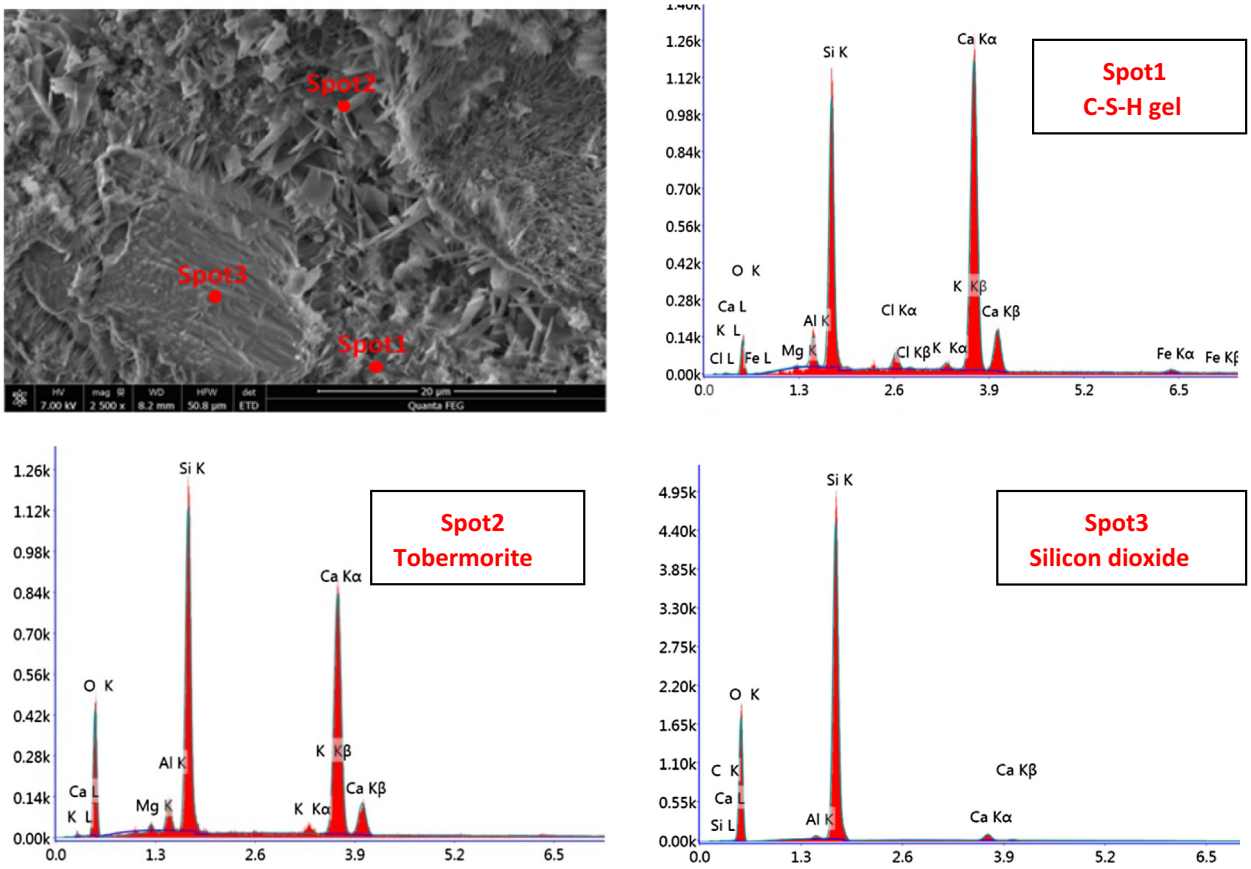

Fig. 8. Predominant phases in AAC sample.

tobermorite, which were mostly contributed to the mechanical property, finally result in weaken of compressive strength [21].

The effect of MSIS suggests that the iron tailing content in AAC should be carefully controlled to achieve the product quality. In addition, the compressive strengths of MSIS 50% samples are instability, therefore, the samples with 40% MSIS were appropriate both on the performance of ACC and the utilization ratio of iron tailing in this study.

3.2.2. Effects of iron tailing fineness

Fig. 7 indicated that the bulk density, compressive strength and specific strength of the varying AAC samples with different iron tailing fineness.

The diagram indicates that the bulk densities of the samples were between 497 kg/m^3 to 512 kg/m^3, by random. Meanwhile, the samples with longer ground iron tailing were better performed on compressive strength, and the specific strength was also keep on increasing, which indicated that finer iron tailings generated better hydrothermal synthesis production structure when the samples were produced at the same foaming process. The mean compressive strength exceeded 2.6 MPa by using over 20 min ground iron tailings, which met the requirements of B05 A2.5 grade in the national standard GB 11968-2006 on the basically mechanical properties.

However, obtaining finer siliceous requires more energy which increases the cost of production. Considering the mechanical property of final products and the energy consumption of milling, the optimal grinding time was 20 min, and the corresponding proportion of particle size under 80 μm is 83.57%.

3.3. Hydrothermal synthesis production analysis

3.3.1. Morphologic (FESEM) and qualitative (EDX)

The morphologic (FESEM) and qualitative (EDX) analysis of the hydration products in T3 AAC sample were shown in Figs. 8, 9 and Table 5. As Fig. 8 shown, the dough-like phase is believed to be weakly crystalline C-S-H gel (spot 1) partly incorporating with Mg, Al, K and Fe, which is generated at the crust of the silicon dioxide (spot 3). The composition of flake-like phase (spot 2) contains a ratio of nCa/n(Si + Al) = 0.821, which is similar to that of tobermorite (0.833) [22].

The morphology of the pores partition in AAC sample (Fig. 9) shown that, long-strip shaped anhydrite interpenetrating in C-S-H gel with tobermorite crystals. The flake-like tobermorite was formed interfingered and overlapped with each other on the C-S-H gel; meanwhile, each C-S-H gel unit is combined through the skeleton formed by tobermorite crystals. The interconnected and cavity microstructure resulted in the high compressive strength, good thermal insulation and heat preservation performance of AAC blocks [23,24].

3.3.2. Mineral constitute (XRD)

The diffraction patterns given in Figs. 10 and 11 were for samples prepared with different MSIS and iron tailing fineness, respectively. As AAC patterns shown, the AAC products mainly composed with tobermorite, anhydrite, hydrogarnet, and some residual minerals including quartz and calcite accompanied by ferric oxide and white mica in minor quantities. The unreacted calcite together with white mica, magnetite phases would become the primary aggregate in the AAC samples [22]. The

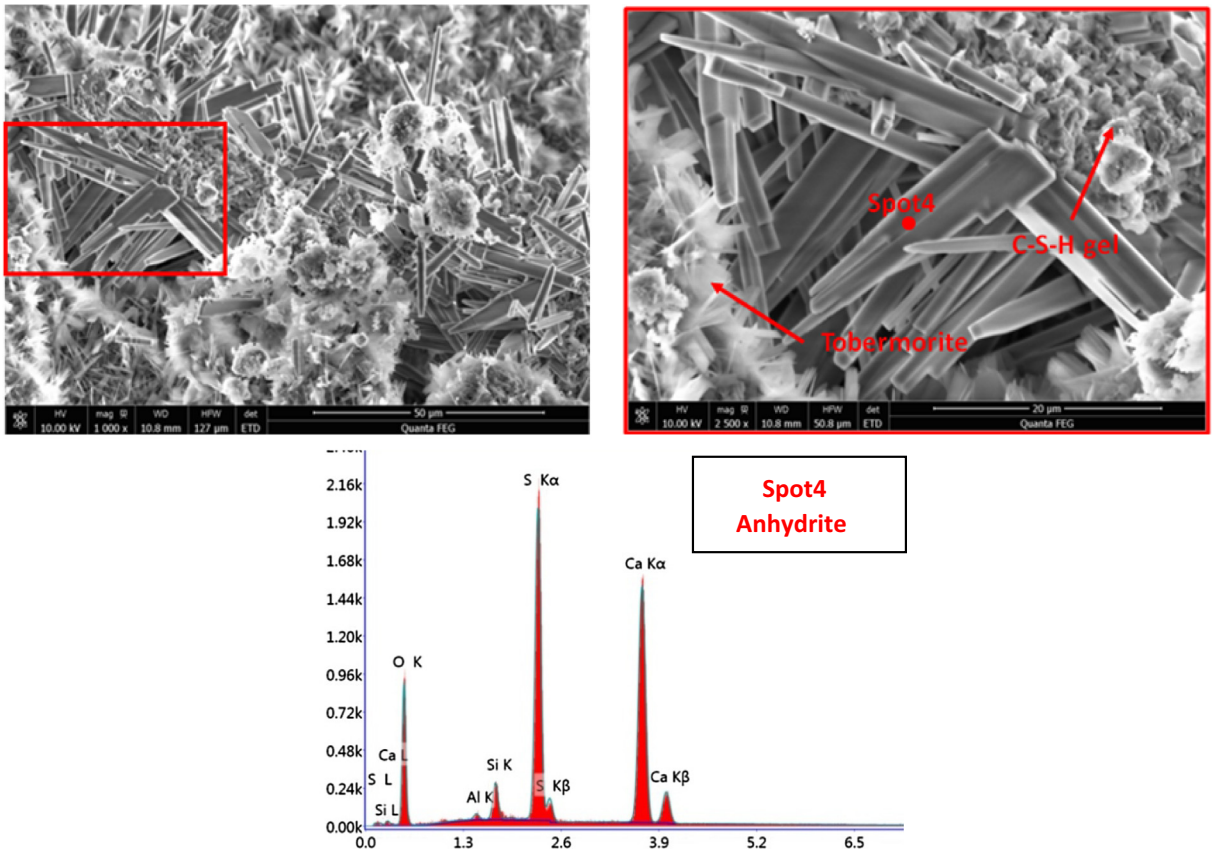

Fig. 9. Anhydrite phase in T3 AAC sample.

Table 5
Qualitative results of EDX.

Element	Spot1 C-S-H gel		Spot2 Tobermorite		Spot3 Silicon dioxide		Spot4 Anhydrite	
	Element wt/%	Atom/%	Element wt/%	Atom/%	Element wt/%	Atom/%	Element wt/%	Atom/%
O	32.55	51.63	46.42	63.69	54.53	67.51	51.33	70.2
Al	1.5	1.41	1.51	1.23	0.45	0.33	0.48	0.39
Si	18.46	16.68	20.55	16.06	42.43	29.93	2.08	1.62
Cl	2.41	1.72	1.62	1	–	–	–	–
K	0.94	0.61	0.88	0.49	–	–	–	–
S	–	–	–	–	–	–	19.24	13.13
Ca	44.14	27.94	25.93	14.2	1.76	0.87	26.87	14.67

broadened "convex closure" in the range of 26–34° indicated that amorphous, weakly crystalline substances, C-S-H gel [21]. The C-S-H gel acted as a binder bonding all components in AAC together to form a good network that resists stress concentration under loading [25,26].

Hydrogarnet was able to precipitate rapidly in a wide temperature range due to massive calcium interaction with the dissolved Si^{4+} and Al^{3+} from iron tailings during the autoclaving [27].

The XRD patterns of AAC samples with different MSIS were shown in Fig. 10 and the parameters of characteristic peaks of the main minerals are presented in Table 6 and Table 7. As shown in Fig. 10 and Table 6, the intensity of the three main characteristics tobermorite peaks, (d, 2θ) = (11.3 Å, 7.8°), (3.08 Å, 28.98°), (2.98 Å, 30.04°), in the diagram of AAC samples diminished gradually with the increasing of MSIS, indicating a decrease of relative amount and crystallinity of tobermorite crystal. This is attributing to the lower SiO_2 content in iron tailing than silicon sand, resulted in less amount of Si^{4+} dissolved from siliceous in alkaline hydrothermal conditions, which restrained the formation of tobermorite, and led to a significant reduction on compressive strength [22].

As some residual minerals in AAC samples, the characteristics peak intensity of white mica (d = 9.93 Å) and calcite (d = 3.03 Å), which were shown in Table 7, intensifies significantly with adding of iron tailings. The phase composition of different MSIS AAC samples presented the same regularity with the influence on mechanical properties.

Fig. 11 and Table 8 indicated the XRD patterns and parameters of AAC sample T8, T3 and T11. It could be informed from intensity value of characteristics peak of tobermorite that the finer of iron tailings have slight negative effect on formation of tobermorite, which was in contrast to the law of mechanical properties change with fineness of iron tailing. This was ascribed to the finer iron tailing resulted in higher degree of reaction and lower crystallinity than that of coarser iron tailing in hydrothermal reaction [28]. Meanwhile, as siliceous of sample T8, T3 and T11 consist of 60% silicon sand with similar particle size distribution and 40% iron tailing with various particle size distributions, the crystal structure

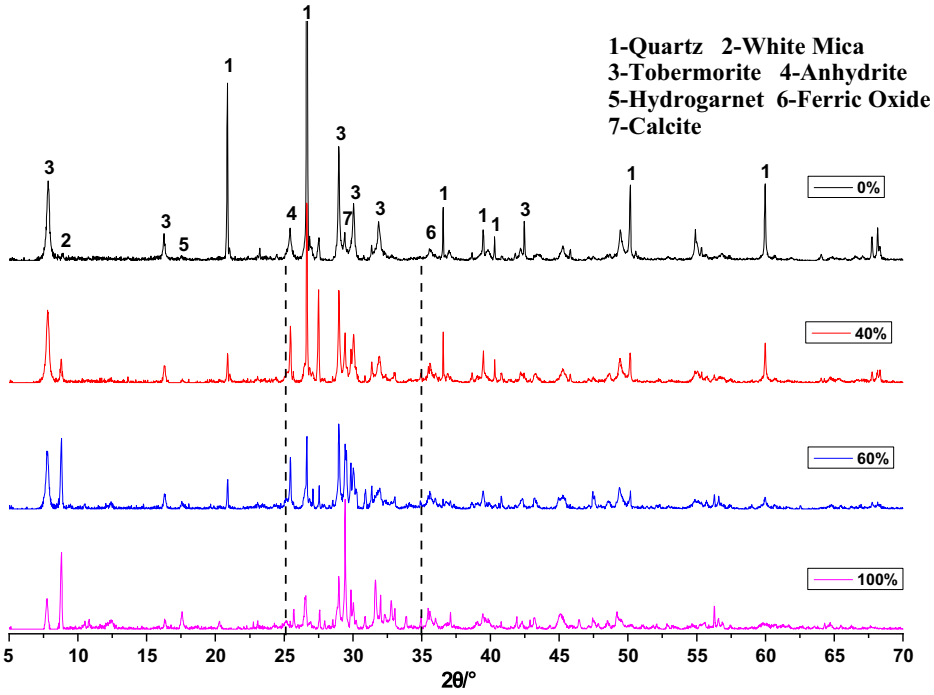

Fig. 10. XRD patterns of AAC samples with different MSIS.

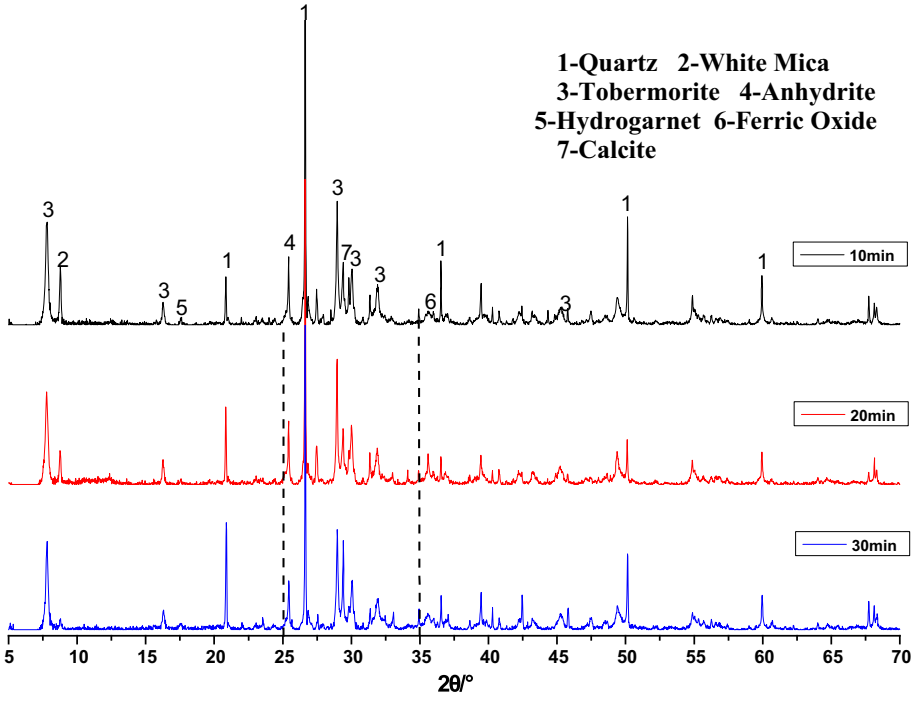

Fig. 11. XRD patterns of AAC samples prepared from different fineness iron tailings.

Table 6
Parameters of tobermorite characteristic peaks of AAC samples with different MSIS.

2θ(°)	11.3 Å				3.08 Å				2.98 Å			
MSIS (%)	0	40	60	100	0	40	60	100	0	40	60	100
Intensity (cps)	3313	2895	2389	1231	4728	3563	3216	1921	2334	1913	1622	1231
FWHM	0.244	0.27	0.258	0.17	0.155	0.168	0.172	0.201	0.212	0.227	0.281	0.138
XS (Å)	351	337	350	594	862	867	958	504	499	310	215	>1000

Table 7
Parameters of white mica and calcite characteristic peaks of AAC samples with different MSIS.

Mineral-2θ(°)	White mica-9.93 Å				Calcite-3.03 Å			
MSIS (%)	0	40	60	100	0	40	60	100
Intensity (cps)	138	866	2687	2967	1018	1824	2400	4345
FWHM	0.089	0.156	0.135	0.112	0.377	0.212	0.216	0.142
XS(Å)	>1000	>1000	>1000	>1000	502	727	511	>1000

Table 8
Parameters of tobermorite and white mica characteristic peaks of AAC samples with different fineness iron tailings.

Mineral-2θ(°)	Tobermorite-11.3 Å			White mica −9.93 Å		
MSIS (%)	10 min	20 min	30 min	10 min	20 min	30 min
Intensity (cps)	3378	2926	2716	1701	993	301
FWHM	0.229	0.253	0.259	0.149	0.154	0.181
XS(Å)	445	378	336	>1000	>1000	990

Table 9
Weight change proportion of the 4 temperature range of Fig. 11.

Temperature Range(°C)	Weight change (%)			
	MSIS-0%	MSIS-40%	MSIS-60%	MSIS-100%
I-(100–470)	−6.24999	−5.31416	−5.30187	−4.41234
II-(470–650)	−0.9391	−0.59535	−0.59372	−0.21623
III-(650–740)	−1.06403	−2.33782	−2.9132	−3.09731
IV-(740–1000)	−0.15331	−0.23289	−0.88013	−0.95457

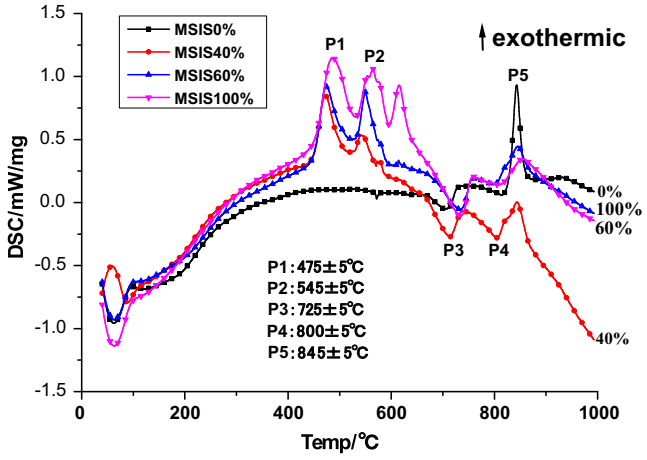

Fig. 12. DSC curves of different MSIS AAC samples.

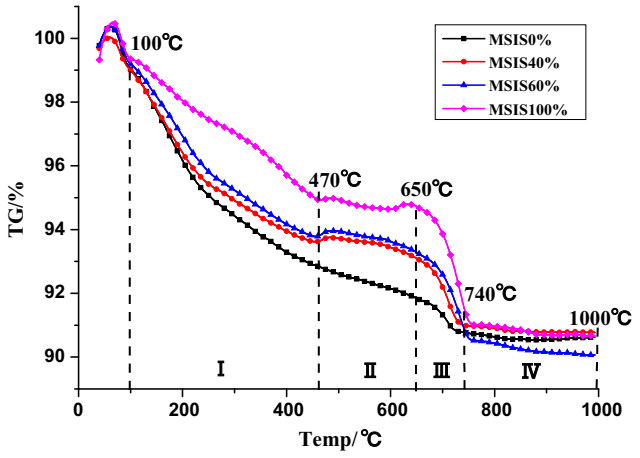

Fig. 13. TG curves of AAC samples with different MSIS.

of tobermorite mostly determined by the component which provides more SiO_2. On the other hand, as MSIS constant at 40%, the decrease of diffraction intensity of the main characteristics peak of white mica (d = 9.93 Å) mainly caused by the finer of iron tailing particles.

3.3.3. Thermal characteristics (DSC-TG)

Based on the morphology and mineralogical analysis results, the hydration products of iron tailing AAC are multiple, therefore, the DSC and TG curves were combined by characteristic of each constituent minerals.

The result of DSC and TG analysis of AAC sample with different MSIS were presented in Figs. 12and 13, respectively. As exothermic peaks P1 and P2 were not appear in the MSIS 0% curve, and considering DSC and TG analysis of iron tailing, P1 and P2 of Fig. 12 were related to the oxidation reaction of organic matter in iron tailings. The slight weight increment in the TG curve at 470 °C may caused by the oxidation of ferric oxide. With further heating, P3 endothermic peaks at 725 ± 5 °C were related to the decomposition of calcite with generating of CaO, and accompanied with obvious weight loss. The endothermic peaks at 800 ± 5 °C were related to the dehydration of xonotlite and transforming into beta-wollastonite (β-wollastonite). The exothermic peaks at 845 ± 5 °C were supposed to be the transforming of dehydrated C-S-H (B) and Al-substituted tobermorite into β-wollastonite with sharp shrinkage [31,32]. Therefore, the DSC analysis presented the similar mineral composition with morphology and XRD analysis of AAC samples.

As shown in Fig. 13, the TG curves of AAC samples could be decompose into 4 stages. Meanwhile, the weight loss proportions were listed in Table 9. Stage I, from 100 °C to 470 °C, which was related to the dehydration of C-S-H (B) and tobermorite transforming into CSH (A), and the weight loss decreased with addition of iron tailing. The reducing weight loss of stage I indicated that the amount of C-S-H (B) and tobermorite were gradually decreased with the increasing of iron tailing, which was coincides with the regularity of Fig. 6. This phenomenon was also in agreement with the result of XRD analysis (Fig. 10). The TG curves flatten out in stage II, which was related to the oxidation reaction of organic matter in iron tailings. As temperature range of stage III, 650–740 °C, related to the decomposition of calcite. In this stage, especially the samples with more addition of iron tailing presented greater reduction on the weight loss. In the last stage, 740–1000 °C, which was corresponding to the transforming of xonotlite and dehydrated C-S-H (B) and tobermorite into β-wollastonite, presented barely distinctions between the different MSIS AAC samples in weight loss.

Figs. 14 and 15 depicted the DSC and TG curves of AAC samples with different fineness iron tailing. As indicated in Fig. 14, the *endo*-exothermic characteristic peaks shown no significant difference between AAC samples prepared with different fineness iron

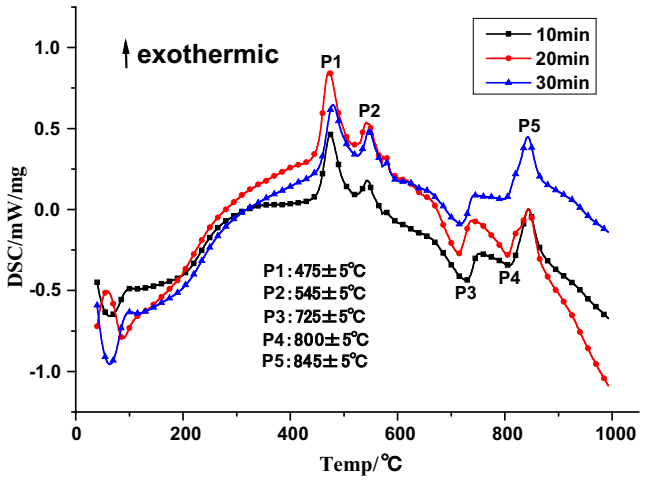

Fig. 14. DSC curves of different milling time iron tailing AAC samples.

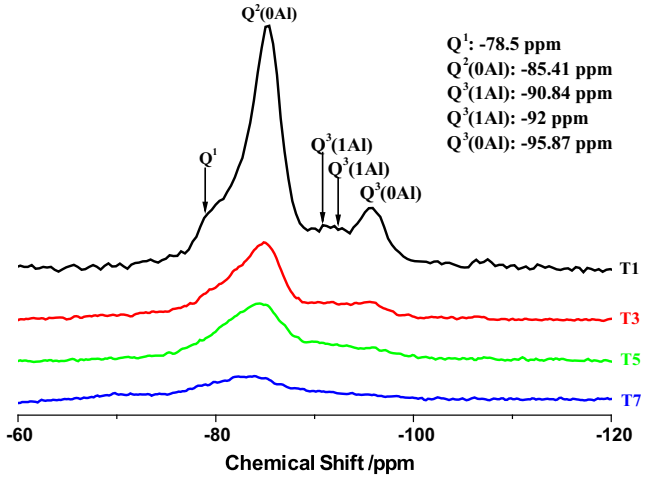

Fig. 16. ^{29}Si NMR spectra of AAC samples.

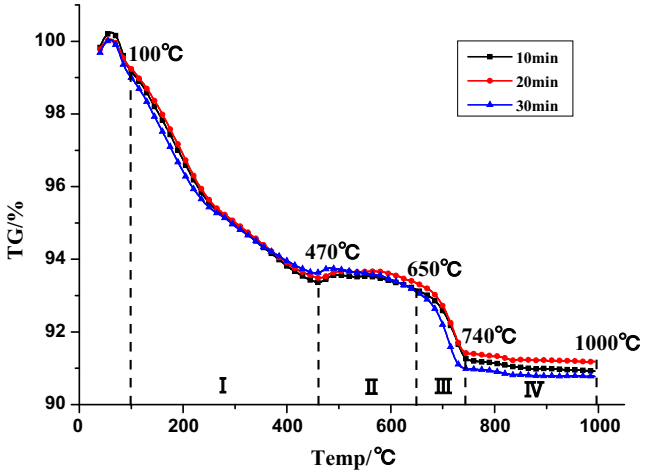

Fig. 15. TG curves of different milling time iron tailing AAC samples.

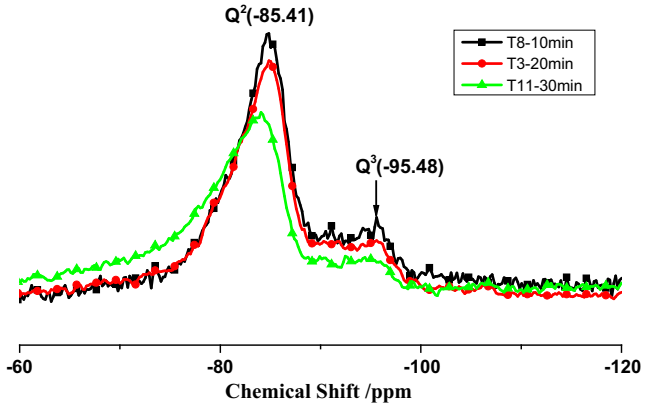

Fig. 17. ^{29}Si NMR spectra from AAC samples with different fineness iron tailing.

Table 10
Weight change proportion of the 4 temperature ranges of Fig. 13.

Temperature Range(°C)	Weight change (%)		
	10 min	20 min	30 min
I-(100–470)	−5.75137	−5.73529	−5.30187
II-(470–650)	−0.25125	−0.16113	−0.59535
III-(650–740)	−1.80657	−1.87331	−2.09132
IV-(740–1000)	−0.42892	−0.28141	−0.23289

tailing. Meanwhile, the TG curves and weight change proportion of the 4 temperature ranges, shown in Table 10, also presented similar features. This was confirmed the result of XRD analysis. It could be seen that the changing on fineness of iron tailing with 40% mass ratio had little effect on hydration products when ingredient is constant. The promotion of mechanical property by finer iron tailing particle size may benefit from the better filling effect of finer unreacted iron tailing, which could strengthen the pore wall in a certain degree.

3.3.4. ^{29}Si nuclear magnetic resonance (NMR)

Figs. 16 and 17 showed the ^{29}Si-NMR spectra of the AAC samples with various MSIS and iron tailing fineness, respectively.

According to widespread use, SiO_4^{4-} units are identified according to their mutual connectivity as Q^n(mAl), where n is the number of shared oxygen atoms with other silicate or aluminate tetrahedra, and m is the number of neighbor aluminate groups [33].

Marks on the peaks show the assignments of resonances with silicon environments

As the XRD analysis demonstrated in Section 3.3.2, tobermorite-11 Å was the dominant phase in AAC samples. Meanwhile, tobermorite without added aluminium exhibit two resonances at −85.7 ppm and −95.7 ppm. These two resonances arise from chain middle groups (Q^2) and branching site (Q^3), respectively, as been suggested by Wieker et al. [34].

As seen in Fig. 16, spectrum of sample T1 shown two easily resolved resonances associated with ^{29}Si in hydration products (mainly C-S-H (B) and tobermorite as indicated by the X-ray patterns). Thus, the most prominent two signals at −85.41 ppm and −95.87 ppm could be assigned to Q^2 (0Al) and Q^3 (0Al) sites in tobermorite-11 Å, respectively. In addition to the broad line around −78.5 ppm was corresponding to Q^1 site in lower crystallinity, amorphous C-S-H. gel. Between the two major signals, there were minor subsidiary peaks. Among them, peaks around −90.84 ppm and −92 ppm may be indicative of Q^3 (1Al) structure state of tobermorite-11 Å, indicating that Al also had substituted in Q^3 units in tobermorite structure [35]. Meanwhile, as the Mg could also participate in the hydrothermal reaction to produce tobermorite, the Ca in tobermorite-11 Å may be substituted by Mg in

iron tailing. Thus, the signal at −90.84 ppm may be caused by the Q^3 (1Al) sites where Mg ions were the linkages between the chains, and the signal at −92 ppm could be assigned to Q^3 (1Al) sites where Ca ions were the linkages [8].

Compared with the intensity of signal at −85.41 ppm assigned to Q^2 (0Al) site, the intensity of signal at −95.87 ppm assigned to Q^3 (0Al) sites was significantly lower, which suggested that the Si-O-Si branching sites between silicate double chains were quite few. On the other hand, the additive of iron tailings had significant adverse effects on the formation of tobermorite-11 Å in the view of intensity. The signal of Q^3 (0Al) site even vanished when the silicon sand was 100% substituted by iron tailings. This consequence is in agreement with the results of compressive strength and XRD analysis.

Evidently, all of the peaks with chemical shifts beyond −95.87 ppm were very low, suggesting most minerals with Q^3 (0Al) and Q^4 (nAl) sites, which were quartz and field spar minerals, have been largely consumed. These seems to be a contradiction between the XRD pattern which shown the highest peak belongs to quartz and the ^{29}Si NMR spectrum which shows very low content of residue quartz in the final AAC samples. This was ascribed to the well crystallinity quartz. Small amounts of quartz can make a very strong peak in the XRD pattern.

The ^{29}Si-NMR spectra of AAC samples from various fineness iron tailings were presented in Fig. 17. It can be seen that the peaks at −85.41 ppm, which is referred to the Q^2 (0Al) site in tobermorite-11 Å obviously broadened with the finer of iron tailings. This phenomenon indicating that the tobermorite group of C-S-H formed using the finer siliceous was of lower crystallinity than that using the coarser siliceous. Thus, as the total amount of calcium silicate hydrates of the AAC samples are approximate according to the TG analysis(Fig. 13) in Section 3.3.3, relatively, more C-S-H(B)-like in character with the finer of siliceous[32]. This is conforming to the results of the research of Norifumi Isu et al. [28]. Meanwhile, as J. Alexanderson [10] expounded in the research of relations between crystallinity and strength of AAC, there is an optimum crystallinity in a certain material system. The lower crystallinity resulting in higher compressive strength may attribute to the exceeding of the optimum crystallinity under the mixture proportion and autoclaving process in this study.

4. Conclusions

In this study the feasibility of using iron tailing additives for the production of AAC has been demonstrated. Based on the work undertaken here, the following conclusions may be drawn:

(1) The increasing of substitution mass ratio of iron tailing has negative effect on the compressive strength of AAC, and the finer of iron tailing can effectively enhance strength of AAC products. The appropriate content and fineness of iron tailing in preparing AAC could be 27–34% mass ratio of the total weight and particle size under 80 μm ⩾ 83.57%, respectively. The recommended mass ratio of dry mixture was the iron tailing: silicon sand: cement: quick lime: $CaSO_4{\cdot}2H_2O$ = 27–34:34–41:8:21:3, with a 60% forming water content and 0.14% Al powder, 14 bars saturated steam pressure autoclaving for 8 h to produce eligible AAC. The products under these conditions were well conformed to B05, A2.5 level of Chinese Autoclaved Aerated Concrete Blocks Standard (GB 11968-2006) in the view of bulk density and strength.

(2) Through the morphology analysis, the hydration products of iron tailing AAC products mainly consist of dense C-S-H gel, flake-like tobermorite and long-strip shaped anhydrite. The results of XRD, DSC analysis demonstrate that the AAC products mainly composed with C-S-H gel, tobermorite, anhydrite, hydrogarnet, and some residual minerals including quartz and calcite accompanied by some organic matters, ferric oxide and white mica in minor quantities.

(3) Comparing the results of XRD, TG and NMR analysis of AAC samples, the increasing of substitution mass ratio of iron tailing obviously reduced the amount of calcium silicate hydrates, including C-S-H (B) and tobermorite. The finer of iron tailing accelerated the decomposition of white mica during the autoclaving process and had slight negative effect on the crystallinity of tobermorite. Meanwhile, it had no obvious effect on the amount of calcium silicate hydrates. Through the NMR analysis, it also could be found that the Al and Mg in iron tailings got into the structure of tobermorite during the hydrothermal reaction.

Acknowledgments

The authors thank Dr Linnv Lv for helpful discussions and comments. Support from the National Technology Support Project of China (Project NO. 2011BAJ03B03) is also gratefully acknowledged.

References

[1] N. Narayanan, K. Ramamurthy, Structure and properties of aerated concrete: a review, Cem. Concr. Compos. 22 (5) (2000) 321–329.
[2] Karakurt Cenk, Kurama Haldun, Topçu Ilker Bekir, Utilization of natural zeolite in aerated concrete production, Cem. Concr. Compos. 32 (1) (2010) 1–8.
[3] Miloš Jerman, Martin Keppert, Jaroslav Výborný, Robert Černý, Hygric, thermal and durability properties of autoclaved aerated concrete, Constr. Build. Mater. 41 (2013) 352–359.
[4] H. Andre, E. Urs, M. Thomas, Fly ash from cellulose industry as secondary raw material in autoclaved aerated concrete, Cem. Concr. Res. 29 (3) (1999) 297–302.
[5] N.Y. Mostafa, Influence of air-cooled slag on physicochemical properties of autoclaved aerated concrete, Cem. Concr. Res. 35 (7) (2005) 1349–1357.
[6] H. Kurama, I.B. Topçu, C. Karakurt, Properties of the autoclaved aerated concrete produced from coal bottom ash, J. Mater. Process. Technol. 209 (2) (2009) 767–773.
[7] W.H. Mirza, S.I. Al-Noury, Utilisation of Saudi sands for aerated concrete production, Int. J. Cem. Compos. Lightweight Concrete 8 (2) (1986) 81–85.
[8] Xiao-yan Huang, Wen Ni, Wei-hua Cui, Zhong-jie Wang, Li-ping Zhu, Preparation of autoclaved aerated concrete using copper tailings and blast furnace slag, Constr. Build. Mater. 27 (2012) 1–5.
[9] Fan Junjie, Cao Deguang, Jing Zhenzi, Zhang Yi, Pu Li, Jing Yani, Synthesis and Microstructure Analysis of Autoclaved Aerated Concrete with Carbide Slag Addition, in: J. Wuhan Univ. Technol. Mater. Sci. 10 (29) (2014) 1005.
[10] J. Alexanderson, Relations between structure and mechanical properties of autoclaved aerated concrete, Cem. Concr. Res. 9 (1979) 507–514.
[11] G.C. Abbate, Understanding autoclaved aerated concrete, Constr. Specif. 57 (6) (2004) 66–74.
[12] S. Zhang, X. Xue, X. Liu, P. Duan, H. Yang, T. Jiang, D. Wang, R. Liu, Current situation and comprehensive utilization of iron ore tailing resources, J. Min. Sci. 4 (2006) 403–408.
[13] A.A. Sirkeci, A. Gül, G. Bulut, F. Arslan, G. Onal, A.E. Yuce, Recovery of Co, Ni, and Cu from the tailings of divrigi iron ore concentrator, Miner. Process. Extr. Metall. Rev. 27 (2) (2006) 131–141.
[14] B. Das, P.S.R. Reddy, V.N. Misra, Recovery of iron values from tailing dumps adopting hydrocyclone and magnetic separation techniques, Austr. Inst. Mining Metal. Pub. Ser. 2 (2002) 285–289.
[15] Chuan meng Yang, Chong Cui, Juan Qin, Xiaoyu Cui, Characteristics of the fired bricks with low-silicon iron tailings, Constr. Build. Mater. 70 (2014) 36–42.
[16] S.K. Das, Sanjay Kumar, P. Ramachandraro, Exploitation of iron ore for the development of ceramic tiles, Waste Manage. 20 (2000) 725–729.
[17] Sujing Zhao, Junjiang Fan, Wei Sun, Utilization of iron ore tailings as fine aggregate in ultra-high performance concrete, Constr. Build. Mater. 50 (2014) 540–548.
[18] F.L. da Silvaa, F.G.S. Araújoa, M.P. Teixeiraa, Study of the recovery and recycling of tailings from the concentration of iron ore for the production of ceramic, Ceram. Int. 40 (2014) 16085–16089.
[19] Wang Yan, Yin Jie, Chen Ji-chun, Peng Chang-qi, Aerocrete made with low silicon tailings of Cheng Chao iron ore mine, J. Wuhan Univ. Technol. Mater. Sci. 15 (2) (2000) 58–62.

[20] S. Osvalda, S. Piero, C. Riccardo, C. Luciano, S. Roberto, Mechanochemical activation of high-carbon fly ash for enhanced carbon reburning, Proc. Combust. Inst. 33 (2011) 2743–2753.
[21] J. Bensted, P. Barnes, Structure and Performance of Cements (2nd Ed.), Spon Press, New York, 2002.
[22] Changlong Wang, Wen Ni, Siqi Zhang, Shuang Wang, Guosheng Gai, Weikang Wang, Preparation and properties of autoclaved aerated concrete using coal gangue and iron ore tailings, Constr. Build. Mater. 104 (2016) 109–115.
[23] E. Bonaccorsi, S. Merlino, A.R. Kampf, The crystal structure of tobermorite 14 Å (Plombierite), a C-S-H phase, J. Am. Ceram. Soc. 88 (3) (2005) 505–512.
[24] Oh Jae Eun, M. Simon Clark, Hans-Rudolf Wenk, Experimental determination of bulk modulus of 14 Å tobermorite using high pressure synchrotron X-ray diffraction, Cem. Concr. Res. 42 (2) (2012) 397–403.
[25] J. Oh, S. Clark, H. Wenk, P. Monteiro, Experimental determination of bulk modulus of 14 Å tobermorite using high pressure synchrotron X-ray diffraction, Cem. Concr. Res. 42 (2012) 397–404.
[26] Li Dezhong, Ni Wen, Hu Zhang Jingwen, ZhangYuyan Hui, Phase transformation of iron ore tailings during autoclaved curing, J. Chin. Cer. Soc. 39 (4) (2011) 708–713.
[27] Z. Zhang, C. Ke, P. Liu, M. Zhong, Analysis and mechanism of hydrogarnets formation and transformation in autoclaved reaction, J. Instr. Anal. 28 (2009) 1008–1011.
[28] Norifumi Isu, Hideki Ishida, Takeshi Mitsuda, Influence of quartz particle size on the chemical and mechanical properties of autoclaved aerated concrete (I) tobermorite formation, Cem. Concr. Res. 25 (2) (1995) 243–248.
[29] N. Yang, W. Yue, The Handbook of Inorganic Metalloid Materials Atlas, Wuhan University of Technology Press, Wuhan, 2000 [in Chinese].
[30] G. Kakali, T. Perraki, S. Tsivilis, E. Badogiannis, Thermal treatment of kaolin: the effect of mineralogy on the pozzolanic activity, Appl. Clay Sci. 20 (2001) 73–80.
[31] Yunliang Zhao, Yimin Zhang, Tiejun Chen, Yongliang Chen, Shenxu Bao, Preparation of high strength autoclaved bricks from hematite tailings, Constr. Build. Mater. 28 (2012) 450–455.
[32] Danielle S. Klimesch, Abhi Ray, Brian Sloane, Autoclaved cement quartz pastes: the effects on chemical and physical properties when using ground quartz with different surface areas Part I: Quartz of wide particle size distribution, Cem. Concr. Res. 26 (9) (1996) 1399–1408.
[33] J. Schneider, M.A. Cincotto, H. Panepucci, ^{29}Si and ^{27}Al high-resolution NMR characterization of calcium silicate hydrate phases in activated blast-furnace slag pastes, Cem. Concr. Res. 31 (2001) 993–1001.
[34] W. Wieker, A.R. Grimmer, A. Winkler, M. Magi, M. Tarmak, E. Lippmaa, Solid-state high-resolution 29Si NMR spectroscopy of synthetic 14 Å, 11 Å and 9 Å tobermorites, Cem. Concr. Res. 12 (1982) 333–339.
[35] Komarneni Sridhar, Roy Rustum, Roy Della M. ^{29}Si and ^{27}Al magic angle spinning nuclear magnetic resonance spectroscopy of Al-substituted tobermorites, J. Mater. Sci. 20 (1985) 4209–4214.